ARTICLE

Quasi-Solid-State Dye-Sensitized Solar Cells with Polymer Gel Electrolyte and Triphenylamine-Based Organic Dyes

Jifu Shi, Shengjie Peng, Juan Pei, Yanliang Liang, Fangyi Cheng, and Jun Chen*

Institute of New Energy Material Chemistry and Enginnering Research Center of Energy Storage & Conversion (Ministry of Education), Chemistry College, Nankai University, Tianjin 300071, People's Republic of China

ABSTRACT We report on the application of a poly(methyl acrylate)/poly(ethylene glycol)-based polymer gel electrolyte and triphenylamine-based metal-free organic dyes in quasi-solid-state dye-sensitized solar cells. The poly(methyl acrylate)/poly(ethylene glycol) hybrid is beneficial to the entrapment of a large volume of liquid electrolyte. At 25 °C, the ionic conductivity and the triiodide ionic diffusion constant of the as-prepared polymer gel electrolyte are 2.1 mS cm^{-1} and 2.3 × 10^{-6} cm^2 s^{-1}, respectively. The quasi-solid-state solar cell sensitized by triphenylamine-based dyes attains an overall energy conversion efficiency of 5.76% at a light intensity of 30 mW cm^{-2}. The presence of poly(ethylene glycol) in the electrolyte obviously increases the conductivity and energy conversion efficiency compared to that without poly(ethylene glycol).

KEYWORDS: quasi-solid-state • dye-sensitized solar cell • electrolyte • triphenylamine • impedance • conductivity

INTRODUCTION

Dye-sensitized solar cells (DSCs) have been intensively studied over the past decade and regarded as an alternative to the conventional inorganic device because of their relatively high efficiency and low cost (1). In the DSCs, the electrolyte and dye play important roles in the determination of the efficiency and long-term stability (2). At present, an acetonitrile-based liquid-state electrolyte is usually used. However, the use of a liquid-state electrolyte always results in encapsulation and long-term stability issues at higher temperatures. It is thus that several attempts have been made to replace the liquid electrolyte with all-solid-state p-type inorganic semiconductors (CuI, CuSCN, etc.) (3, 4), organic hole-transport materials such as triarylamine- or poly(thiophene)-based derivatives (5, 6), and succinonitrile-based plastic crystal electrolytes (7).

Nevertheless, the energy conversion efficiency of the all-solid-state DSCs is lower mainly because of the poor mobility of the charge carriers in the electrolytes and the imperfect contact interface between the electrolyte and the dye-covered nanocrystalline TiO_2 layers (8). On the contrary, the polymer gel electrolytes can improve these contacts and can simply be fabricated (9−11). The first polymer gel electrolyte for DSCs reported in 1995 was prepared by gelation of the liquid-state electrolyte with poly(acrylonitrile) (12). Afterward, a series of polymers and polymer hybrids such as poly(vinylidene fluoride-*co*-hexafluoropropylene), poly(methyl acrylate) (PMA), poly(acrylic acid)/poly(ethylene glycol) (PEG), and poly(acrylamide)/PEG were employed to fabricate the quasi-solid-state DSCs with satisfactory conversion efficiency, making the DSCs viable for practical application (2, 13−15). In polymer hybrids, the presence of PEG can increase the absorbent ability for liquid electrolytes, consequently improving the ionic conductivity (14, 15). In addition, PEG can interact with TiO_2 through Ti ← O bonds and suppress back electron transfer from TiO_2 to I_3^- at the TiO_2/electrolyte interface, which is beneficial to the improvement of the open-circuit voltage (V_{oc}) (16). On the other hand, PMA has ester groups on its polymer chain and can form a homogeneous hybrid without phase disengagement by intermolecular interaction with PEG in a suitable ratio. Thus, it is expected that the PMA/PEG hybrid can entrap a large amount of liquid electrolyte and possess moderate ionic conductivity and good chemical stability, thus further improving the photovolataic performance of the PMA-based quasi-solid-state DSCs.

Another key part of DSCs is the dye. DSCs based on ruthenium complexes have exhibited the highest energy conversion efficiency, while metal-free organic dyes have also attracted increasing interest in recent years because of their high molar extinction coefficient (17), diversity of molecule structures, simple synthesis, and low cost (18). Moreover, the higher molar extinction coefficient of organic dyes in the visible region allows light harvesting to be accomplished within thinner photoanodes (17, 19). Thin TiO_2 films enable a high electron collection ratio, making it possible to assemble high-efficiency quasi-solid-state DSCs (20). However, to the best of our knowledge, these types of solar cells with metal-free organic dyes and a hybrid polymer gel electrolyte have been seldom studied. Our group has reported a series of metal-free triphenylamine-based organic dyes (21−23). Among them, TPAR4 and TC4 (shown in Figure 1) with a liquid-state electrolyte have exhibited

* Corresponding author. Fax: (86) 22-2350-6808. E-mail: chenabc@nankai.edu.cn.

Received for review January 17, 2009 and accepted March 16, 2009

DOI: 10.1021/am9000375

Published on Web 04/13/2009

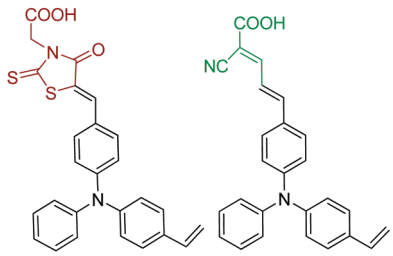

FIGURE 1. Molecular structures of triphenylamine-based dyes TPAR4 and TC4. The different parts are marked by different colors.

considerable energy conversion efficiency of 5.84% and 4.82%, respectively (21, 22). As an extended study, it would be valuable to investigate the photovoltaic performance of these two organic dyes in combination with the polymer gel electrolyte. Therefore, in the present study, we report, for the first time, the preparation and application of a PMA/PEG hybrid gel electrolyte to construct quasi-solid-state DSCs with metal-free dyes of TPAR4 and TC4.

EXPERIMENTAL SECTION

Materials. All reagents used were of analytical grade. The organic dyes TPAR4 and TC4 were synthesized according to refs 21 and 22, respectively. TiO_2 powder (P25, Degussa AG of Germany) consists of 30 wt % rutile and 70 wt % anatase. Conductive glass of fluorine-doped SnO_2 (FTO; 20 Ω sq^{-1}) was purchased from Wanyelong Co. of China. H_2PtCl_6 was supplied by Shanghai Xingao Chemical Reagent Co. Surlyn film (25 μm) was purchased from Heptachroma of China. Other reagents were purchased from Jinhua Co. of China.

Preparation of a Polymer Hybrid and a Polymer Hybrid-Based Gel Electrolyte. The fabrication process of a polymer gel electrolyte is shown in Figure 2a. In a typical preparation, ammonium persulfate (polymerization initiator, 1 wt % methyl acrylate) was dissolved in PEG-400 (4 g) at room temperature. Then, the mixture was added into distilled methyl acrylate (7.26 g) under vigorous stirring at 70−75 °C in a nitrogen atmosphere. After polymerization, a homogeneous mixture was formed (Figure 2b). The content of PEG in this hybrid is 35 wt % [PMA/PEG (65/35)]. In the meantime, the organic solvent was obtained by mixing ethylene carbonate (EC) and propylene carbonate (PC) with different mass ratios. Predetermined amounts of LiI and I_2 (10 mol % of LiI) were dissolved in the binary organic solvent mixture. After that, 27 wt % PMA/PEG (65/35) hybrid was added into the above solution. Finally, the resulting mixture was heated at 80 °C under vigorous stirring until no solid was observed. After naturally cooling down to room temperature, a uniform motionless polymer gel electrolyte was obtained (Figure 2c).

Assembly of DSCs. The FTO glass was immersed in a 50 mM $TiCl_4$ aqueous solution at 70 °C for 0.5 h (24). The TiO_2 paste used to prepare the TiO_2 film consists of 16.2 wt % P25 and 4.5 wt % ethyl cellulose in terpineol. A layer of TiO_2 paste was coated on the pretreated FTO by screen-printing and then dried for 5 min at 125 °C, following the literature procedure (25). The thickness of the TiO_2 films was controlled by repetition of the screen-printing. The prepared TiO_2 films were calcined at 450 °C for 30 min under flowing oxygen to completely oxidize the organic materials such as ethyl cellulose and terpineol in the paste. After cooling to room temperature, the films were treated with a 50 mM $TiCl_4$ aqueous solution and recalcined at 450 °C for 30 min. This treatment with $TiCl_4$ can improve the short-circuit photocurrent density (J_{sc}) as well as the open-circuit voltage (V_{oc}) of the DSCs (26). The surface profiling of the obtained films was measured by a Dektak-150 surface profiler. Figure 3a shows a three-dimensional surface image of the porous and rough TiO_2 film prepared by screen-printing four times. The average roughness (R_a) is measured to be 2.58 μm, and the thickness is around 8 μm, which is further confirmed by the two-dimensional image in Figure 3b.

The as-prepared TiO_2 films were immersed in a dry methanol solution of the organic dyes (all dye solutions had a standard concentration of 3×10^{-4} M) and kept at room temperature for 24 h in the dark to adsorb the dyes on the surface of the TiO_2 film. The Pt counter electrodes were prepared by spin-coating a H_2PtCl_6 solution (50 mM isopropyl alcohol) onto FTO glass and sintering at 390 °C for 0.5 h. Two types of DSCs were fabricated in this work. The first type of DSCs was assembled as follows: The dye-covered TiO_2 electrode and the Pt counter electrode were separated by adhesive tape. The electrolyte was dripped on the dye-covered TiO_2 film at 80 °C. The two electrodes were clipped together for photovoltaic and electrochemical measurements. The second type of DSCs for the long-term stability test (at 60 °C for 1000 h in the dark) was sealed by a Surlyn film (27). The two electrodes were separated by a Surlyn film hot-melt ring and sealed by heating. The internal space was evacuated, and the electrolyte was injected from the predrilled hole on the counter electrode at 80 °C. Finally, the electrolyte introduction hole was sealed with a Surlyn sheet under a thin glass cover by heating. The rigorous sealing of DSCs for the stability test is necessary because the electrolyte becomes flexible at higher temperature (28).

Instruments and Measurements. The thermograms were measured with a Mettler Toledo DSC1/500/352 at a heating rate of 10 °C min^{-1}. The microstructures of the as-prepared polymer and polymer hybrid were investigated by scanning electron microscopy (SEM; JEOL JSM-6700F field emission). The samples for SEM were prepared by loading the polymer gel electrolytes into water to shrink the absorbed liquid electrolyte and PEG and then freeze-drying prior to SEM observation. Impedance, voltammetry, and open-circuit voltage decay (OCVD) experiments were performed on a computer-controlled PARSTAT 2273 Advanced Electrochemical System (Princeton Applied Research). The impedance measurements were carried out in the frequency range from 100 kHz to 10 mHz with an amplitude of 10 mV.

The ionic conductivity and temperature dependence of the polymer gel electrolyte were determined by impedance measurements. The electrolyte was sandwiched between two mirror-finished stainless steel electrodes using a Teflon ring spacer in a constant-volume cylindrical cell and was sealed with paraffin in the glovebox. The sealed cell was maintained at various constant temperatures for at least 1 h prior to each measurement. The conductivity was calculated from the bulk resistance R_b. The cell constant was determined by calibration before and after measurement with a 0.1 M KCl aqueous solution. The diffusion constant of I_3^- was measured by cyclic voltammetry with a sandwich cell composed of two platinized FTO glass electrodes separated by a 50 μm spacer (schematically illustrated in Figure S1 in the Supporting Information). The scan rate was 0.01 V s^{-1}.

The photocurrent density−voltage characteristics of DSCs were measured by a Keithley 2400 digital source meter controlled by a computer. A 500 W xenon lamp served as the sunlight simulator in combination with a band-pass filter (400−800 nm) to remove UV and IR radiation. Further calibration was carried out by a USB4000 plug-and-play miniature fiber-optic spectrometer (Ocean Co.).

RESULTS AND DISCUSSION

Differential Scanning Calorimetry Analysis of the Polymer Hybrid. The miscibility of the polymer

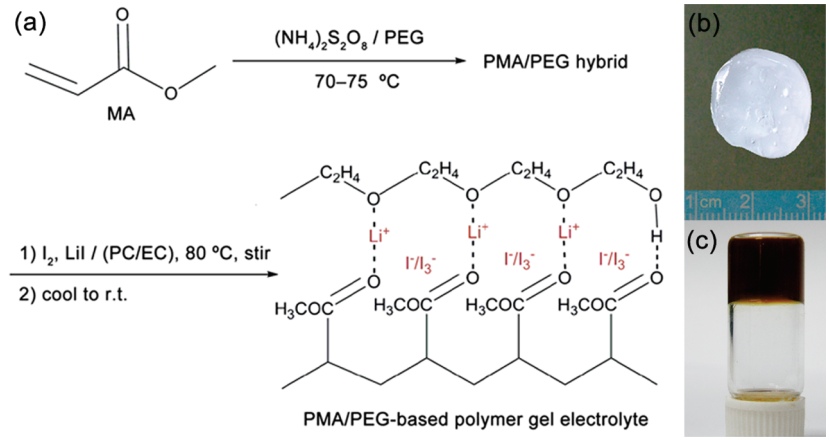

FIGURE 2. (a) Illustration of the preparation process of the PMA/PEG-based polymer gel electrolyte. Photographs of (b) a PMA/PEG (65/35) hybrid and (c) a PMA/PEG-based polymer gel electrolyte in the glass bottle.

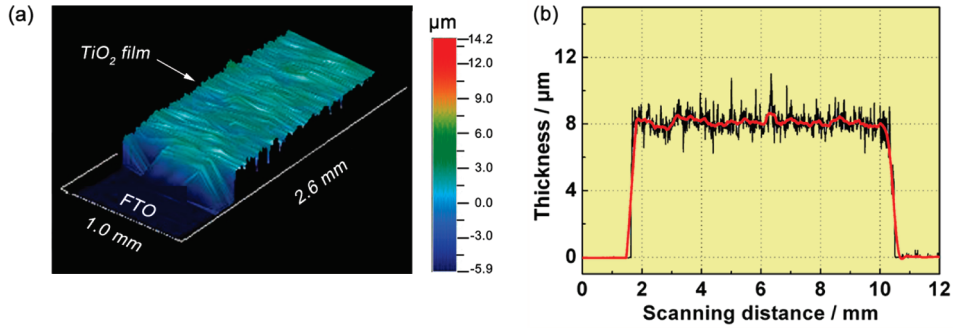

FIGURE 3. (a) Three-dimensional and (b) two-dimensional surface profiling of the TiO_2 film prepared by screen-printing four times. In part b, the red line is the smoothing line of the measured result (black line).

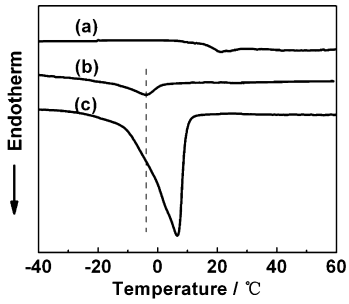

FIGURE 4. Differential scanning calorimetry thermograms of (a) PMA, (b) PMA/PEG (65/35), and (c) PEG with a heating rate of 10 °C min^{-1}.

hybrid was studied by differential scanning calorimetry. The curve a in Figure 4 is the thermogram of pure PMA, showing a glass transition temperature (T_g) of 18 °C. The thermogram of pure PEG shown in curve c displays a melting temperature (T_m) of 6 °C. Curve b is the thermogram of PMA/PEG (65/35). It can be seen that T_g disappears for the PMA/PEG hybrid and that T_m is decreased to −4 °C because of the intermolecular interaction between PMA and PEG. The disappearance of T_g together with the decrease of T_m indicates that the hybrid is miscible (29).

Optimization and Characterization of the Polymer Gel Electrolyte. The polymer gel electrolyte was optimized by adjusting the mass ratio of EC/PC and the concentration of LiI. The binary organic mixture containing EC and PC is used as the solvent of the polymer gel electrolyte. Figure 5 indicates that the content of EC and the concentration of LiI have a great influence on the ionic conductivity of the electrolyte. EC has a high dielectric constant (ϵ_r = 90 at 40 °C), which is beneficial to the formation of free salvation ions of the lithium salt and affords more charge carriers (30). The ionic conductivity first increases and then decreases as the EC content increases from 15 to 90 wt %, achieving the maximum value at 80 wt % (Figure 5a). When the content of EC exceeds 80 wt %, the ionic conductivity decreases because of crystallization of EC (T_m = 37 °C). The solvent PC with a relatively low dielectric constant (ϵ_r = 65 at 25 °C) can solve EC to form a binary organic solvent mixture. The mass ratio of EC/PC is fixed at 8/2 in this study.

Figure 5b presents the variation of the ionic conductivity as a function of the concentration of LiI. The ionic conductivity attains a maximum of 2.1 mS cm^{-1} at a concentration of 0.6 M. When the concentration of LiI is lower, an increased LiI concentration can supply more charge carriers, hence resulting in larger ionic conductivity. At concentrations higher than 0.6 M, LiI cannot be ionized completely and forms associated ions. The mobility of the associated ions is restrained and contributes less to the ionic conductivity (28). Thus, the optimal polymer gel electrolyte is composed of a 27 wt % PMA/PEG (65/35) hybrid, 0.6 M LiI, and 0.06 M I_2 in the mixed solvent of EC/PC with a mass ratio of 8/2.

In order to illustrate the effect of PEG, PMA/PEG-based polymer gel electrolytes with different PEG contents (0, 20,

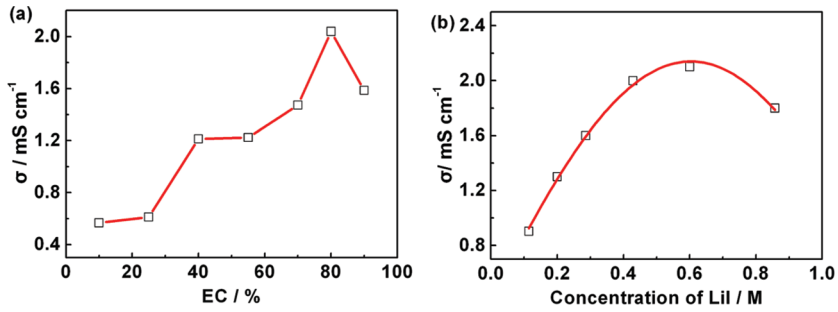

FIGURE 5. Effect of (a) the EC content and (b) the LiI concentration on the ionic conductivity of the polymer gel electrolyte.

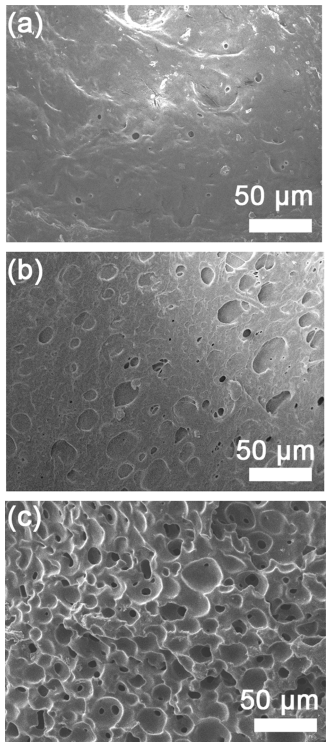

FIGURE 6. SEM images of the polymer samples after liquid electrolyte extraction: (a) PMA without PEG; (b) PMA/PEG (80/20); (c) PMA/PEG (65/35).

and 35 wt %) in the hybrids were prepared. Figure 6 shows the SEM images of cross sections of swollen polymers after electrolyte extraction from the polymer matrix. It can be clearly observed that all samples display porous structure and that the size and quantity of the pores in the polymer correlate with the content of PEG. The formation of pores is possibly due to shrinkage of the polymer matrix after extraction of PEG and the liquid electrolyte (14) during the sample preparation process for SEM measurement. The numerous pores existing in the polymer reflect the favorable capability of the hybrid polymer for entrapping liquid electrolyte. On the basis of the SEM results, the hybrid PMA/PEG (65/35) was selected to prepare the polymer gel electrolyte in this work.

Figure 7 shows the temperature dependence of the ionic conductivity of the polymer gel electrolytes. At 25 °C, the ionic conductivity of the PMA/PEG-based polymer gel electrolyte is 2.1 mS cm^{-1} and increases with temperature because transportation of the ions becomes faster at higher

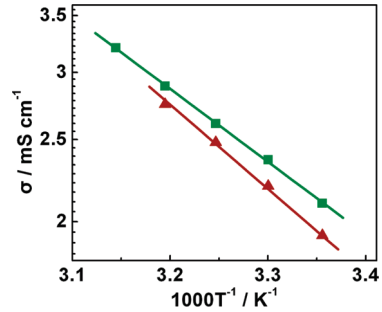

FIGURE 7. Temperature dependence of the ionic conductivity of the polymer gel electrolytes containing 27 wt % of PMA/PEG (green squares) or pure PMA (red triangles), 0.6 M LiI, and 0.06 M I_2 in a mixed solvent of EC/PC with a mass ratio of 8/2.

temperature. The data in Figure 7 can be fitted well by the Arrhenius equation (eq 1):

$$\sigma(T) = A \exp\left(\frac{-E_a}{k_B T}\right) \quad (1)$$

where A is a constant, E_a is the activation energy, k_B is Boltzmann's constant, and T is the absolute temperature. The activation energy of the PMA/PEG-based electrolyte is calculated to be 16.94 kJ mol^{-1}, which is comparable to the value reported for polymer gel electrolyte systems (31). It can be seen from Figure 7 that the presence of PEG can increase the ionic conductivity. At 25 °C, the ionic conductivity of the PMA-based polymer gel electrolyte is 1.9 mS cm^{-1}, lower than that of the PMA/PEG-based electrolyte. The corresponding activation energy is 18.99 kJ mol^{-1}, which is larger than that of the PMA/PEG-based hybrid polymer gel electrolyte and thus indicates inferior ionic conduction.

Figure 8a shows the cyclic voltammograms of the polymer gel electrolyte measured at different temperatures. The characteristic diffusion-limiting currents, due to the transport of the ionic carriers from one electrode to the other through the whole electrolyte, are observed at both positive and negative potentials. Because of the large excess of I^- in the electrolyte, the current is mainly limited by the diffusion of I_3^- (32, 33). It is known that the diffusion-limiting current density, J_{lim}, is proportional to the diffusion constant of I_3^-, D_{app}:

$$J_{lim} = \frac{2nFC_0D_{app}}{d} \quad (2)$$

where $n = 2$ is the electron-transfer number required for the reduction of triiodide to iodide, C_0 is the bulk concentration of the triiodide ions, d is the distance between two elec-

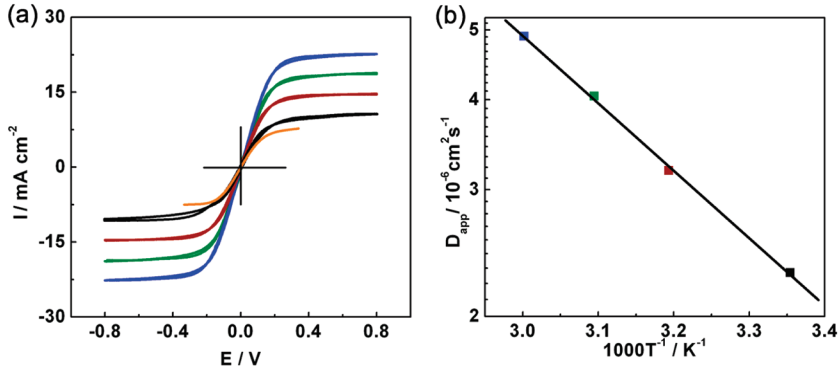

FIGURE 8. (a) Diffusion-limiting currents and (b) diffusion constant of I_3^- at different temperatures for the PMA/PEG-based polymer gel electrolyte (25 °C, black; 40 °C, red; 50 °C, green; 60 °C, blue). For comparison, the diffusion-limiting current of the PMA-based polymer gel electrolyte is also depicted in part a (25 °C, orange).

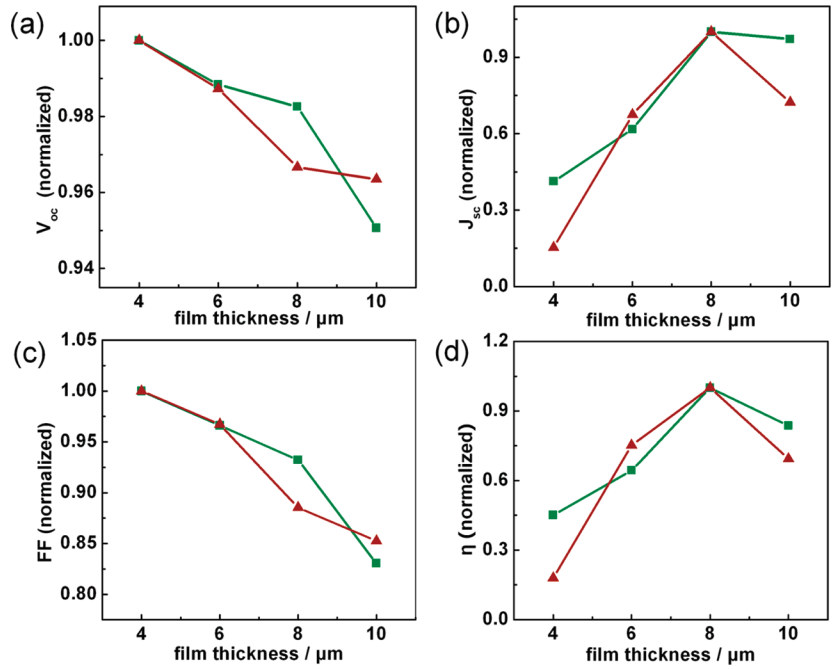

FIGURE 9. Normalized photovoltaic performance of quasi-solid-state solar cells sensitized by TPAR4 (red triangles) and TC4 (green squares) as a function of the nanocrystalline TiO_2 film thickness: (a) open-circuit voltage; (b) short-circuit photocurrent density; (c) fill factor; (d) energy conversion efficiency.

trodes, and F is Faraday's constant. Considering that all of the I_2 added to the electrolyte is converted to I_3^- ($C_0 = 0.06$ M) (33), the D_{app} values of I_3^- at different temperatures are yielded. For the PMA/PEG-based electrolyte, D_{app} is 2.3×10^{-6} cm^2 s^{-1} at 25 °C and increases to 4.9×10^{-6} cm^2 s^{-1} at 60 °C. The temperature dependence of D_{app} can also be described by the Arrhenius equation (eq 1), as shown in Figure 8b (34). For the pure PMA-based polymer gel electrolyte, the J_{lim} value is lower than that of the PMA/PEG-based polymer gel electrolyte (Figure 8a), and the determined D_{app} is 1.7×10^{-6} cm^2 s^{-1} at 25 °C, which is also lower than that of the hybrid gel electrolyte.

Photovoltaic Performance of Quasi-Solid-State Solar Cells Sensitized by TPAR4 and TC4. For the quasi-solid-state DSCs with the low-fluidity electrolyte, the electron collection yield is low because of the short electron diffusion length in the TiO_2 film (35, 36). Reducing the thickness of the TiO_2 film permits more electrons to be collected by the FTO before recombination by triiodide ions in the electrolyte (19, 36). However, a thinner TiO_2 film would incur a lower amount of adsorbed dye and limited absorption of incoming light. Organic dyes with a high molar extinction coefficient help to compensate for the lower optical incidence depth of the thin photoanode (19). At λ_{max}, the molar extinction coefficients of TPAR4 and TC4 are 36 400 (461) and 26 900 M^{-1} cm^{-1} (425 nm), respectively (21, 22), which are much higher than those of the ruthenium complexes such as N3 (14 200 M^{-1} cm^{-1} at 538 nm) and N719 (14 700 M^{-1} cm^{-1} at 535 nm) (37). Hence, it is anticipated that TPAR4 and TC4 would be beneficial for application in quasi-solid-state DSCs. In this study, we employ the metal-free organic dyes TPAR4 and TC4 and the PMA/PEG hybrid polymer gel electrolyte to construct quasi-solid-state DSCs.

Figure 9 depicts the correlation between the nanocrystalline TiO_2 film thickness and the photovoltaic performance of the DSCs assembled with the PMA/PEG hybrid polymer gel electrolyte and TPAR4 or TC4. The thickness of the TiO_2 film has a similar effect on the photovoltaic parameters,

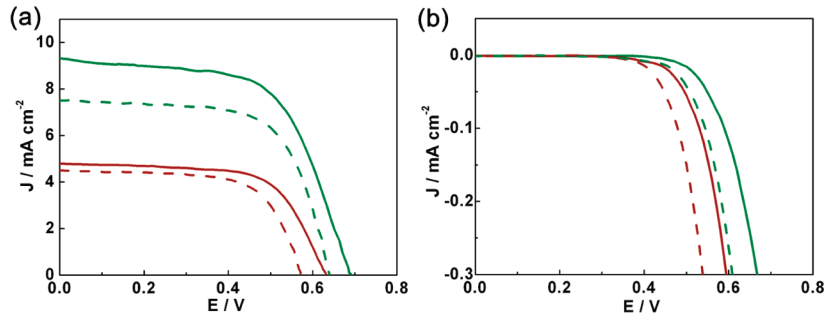

FIGURE 10. (a) Photocurrent density−voltage curves of cell A (red line), cell B (green line), cell C (red dashed line), and cell D (green dashed line) illuminated at a light intensity of 80 mW cm^{-2} and (b) dark current.

Table 1. Detailed Photovoltaic Performance Parameters of V_{oc}, J_{sc}, FF, and η under Various Light Intensities

	light intensity/mW cm^{-2}	V_{oc}/V	J_{sc}/mA cm^{-2}	FF	η/%
cell A	30	0.602	1.7	0.69	2.35
	50	0.618	2.9	0.67	2.40
	80	0.633	4.8	0.65	2.47
	100	0.640	6.3	0.60	2.42
cell B	30	0.661	3.9	0.67	5.76
	50	0.676	5.8	0.65	5.10
	80	0.687	9.3	0.59	4.71
	100	0.691	10.5	0.52	3.77
cell C	80	0.571	4.5	0.67	1.72
cell D	80	0.640	7.5	0.66	3.17

including the normalized open-circuit voltage (V_{oc}; Figure 9a), short-circuit photocurrent density (J_{sc}; Figure 9b), fill factor (FF; Figure 9c), and energy conversion efficiency (Figure 9d), for both the TPAR4- and TC4-based cells. It can be observed that V_{oc} and FF decrease with an increase in the film thickness while the J_{sc} curve displays a volcano shape. The increase of the film thickness can augment the surface area of the photoanode and provide additional charge-recombination sites, consequently lowering their quasi-Fermi level and reducing V_{oc} (19, 36). The decrease of FF with increasing thickness is mainly ascribed to the increased transport resistance of electrons in the TiO_2 particles (19, 33). The maximum η value is attained at a film thickness of 8 μm, which is thinner than that of DSCs assembled with the same dye and liquid-state electrolyte (optical thickness of 14 μm; see Figure S2 in the Supporting Information). Thus, the TiO_2 film thickness of these quasi-solid-state DSCs is optimized as 8 μm.

The photocurrent density−voltage (I−V) curves of the PMA/PEG-based quasi-solid-state solar cells sensitized by TPAR4 (cell A) and TC4 (cell B) illuminated at a light intensity of 80 mW cm^{-2} and in the dark are displayed in Figure 10. For comparison, I−V curves of the pure PMA-based quasi-solid-state solar cells sensitized by TPAR4 (cell C) and TC4 (cell D) measured under the same conditions are also presented in Figure 10. The detailed photovoltaic performance parameters of V_{oc}, J_{sc}, FF, and η under various light intensities are summarized in Table 1. For both dyes, the presence of PEG can obviously improve the photovoltaic performance in terms of increased V_{oc}, J_{sc}, and η, as compared to that of the pure PMA-based electrolyte.

As mentioned above, PEG can be adsorbed onto the TiO_2 surface through Ti ← O bonds and can suppress back electron transfer from TiO_2 to I_3^- (16), consequently raising the quasi-Fermi level of the conduction band electrons in the TiO_2 film and increasing V_{oc}. The increase of J_{sc} is due to the improvement of σ and D_{app}, as shown in Figures 7 and 8. As a result, the η value is improved from 1.72% (cell C) to 2.47% (cell A) for a TPAR4-sensitized solar cell and from 3.17% (cell D) to 4.71% (cell B) for a TC4-sensitized solar cell. The dark current is generally used to estimate the extent of back electron transfer (38). The suppression effect of PEG on back electron transfer can be clearly seen from the dark current in Figure 10b. For both cells containing PEG in the electrolyte, the dark currents are remarkably lower than those without PEG at the same potential.

It should be noted that TPAR4 and TC4 exhibit different photovoltaic performances in the assembled PMA/PEG-based quasi-solid-state solar cells (Figure 10 and Table 1). For cell B, a more negative lowest unoccupied molecular orbital level of dye and a lower back reaction rate at the TiO_2/electrolyte interface between the injected electrons and I_3^- together result in higher J_{sc} as well as V_{oc} (discussed in the Supporting Information). The OCVDs and electrochemical impedance spectroscopy (EIS) analysis showed that cell B exhibited the longer electron lifetime and that the TiO_2 conduction band edge negatively shifted (25 mV) because of adsorption of TC4. These results further explained the superior photovoltaic performance of cell B to that of cell A (Figures S3−S5 in the Supporting Information).

Because the quasi-solid-state solar cells assembled with TC4 and the PMA/PEG-based hybrid polymer gel electrolyte (cell B) show the best photovoltaic performances, we further test their long-term stability following previously reported procedures (27). Cell B was sealed by Surlyn films and stored at 60 °C for 1000 h in the dark. Figure 11 presents the evolution of the conversion efficiency of the sealed cell. The conversion efficiency increased in the beginning stage because of the increase of J_{sc}, which was caused by penetration of the electrolyte through the dye-coated nanoporous TiO_2 electrode (14). After a stabilizing period, the conversion efficiency almost retained its initial value for 1000 h at the testing temperature of 60 °C. The considerable efficiency and excellent long-term stability of cell B reveal that the development of this type of organic-dye-sensitized quasi-solid-state solar cell is promising for commercial applications.

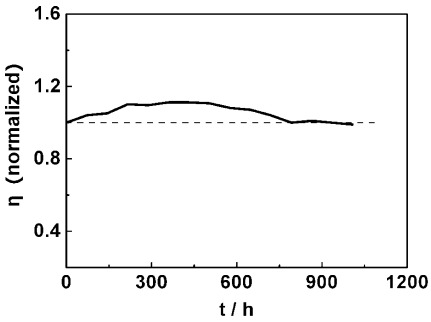

FIGURE 11. Evolution of the conversion efficiency of the quasi-solid-state DSC assembled with TC4 and the PMA/PEG hybrid polymer gel electrolyte. The cell is stored at 60 °C for 1000 h in the dark.

CONCLUSIONS

Quasi-solid-state DSCs were successfully fabricated using the PMA/PEG-based polymer gel electrolyte and triphenylamine-based organic dyes TPAR4 and TC4. The PMA/PEG hybrid polymer gel is beneficial to the entrapment of a large volume of liquid electrolyte. The electrolyte gelatinized by the hybrid PMA/PEG exhibits considerable ionic conductivity and a triiodide ionic diffusion constant. By optimization of the electrolyte composition and TiO_2 film thickness, the fabricated quasi-solid-state solar cells sensitized by TC4 achieve an overall energy conversion efficiency of 5.76% at a light intensity of 30 mW cm^{-2}. The presence of PEG in the electrolyte is found to obviously increase the ionic conductivity and the energy conversion efficiency. The high efficiency and excellent long-term stability of the quasi-solid-state DSCs assembled with metal-free organic dye TC4 and the PMA/PEG hybrid gel electrolyte indicate that they are promising for industrialization.

Acknowledgment. This work was supported by the Programs of National 973 (2005CB623607) and Tianjin High-Tech (07ZCGHHZ00700).

Supporting Information Available: Schematic illustration of the electrochemical cell used for the measurement of the diffusion-limiting current and the influence of the film thickness on the photovoltaic performance parameters of liquid-state solar cells, OCVDs, and EIS analysis. This material is available free of charge via the Internet at http://pubs.acs.org.

REFERENCES AND NOTES

(1) Grätzel, M. *J. Photochem. Photobiol. A* **2004**, *164*, 3–14.
(2) Wang, P.; Zakeeruddin, S. M.; Moser, J. E.; Nazeeruddin, M. K.; Sekiguchi, T.; Grätzel, M. *Nat. Mater.* **2003**, *2*, 402–407.
(3) Meng, Q. B.; Takahashi, K.; Zhang, X. T.; Sutanto, I.; Rao, T. N.; Sato, O.; Fujishima, A. *Langmuir* **2003**, *19*, 3572–3574.
(4) O'Regan, B.; Lenzmann, F.; Muis, R.; Wienke, J. *Chem. Mater.* **2002**, *14*, 5023–5029.
(5) Bach, U.; Lupo, D.; Comte, P.; Moser, J. E.; Weissörtel, F.; Salbeck, J.; Speritzer, H.; Grätzel, M. *Nature (London)* **1998**, *395*, 583–585.
(6) Fukuri, N; Masaki, N.; Kitamura, T.; Wada, Y.; Yanagida, S. *J. Phys. Chem. B* **2006**, *110*, 25251–25258.
(7) Dai, Q.; MacFarlane, D. R.; Howlett, P. C.; Forsyth, M. *Angew. Chem., Int. Ed.* **2005**, *44*, 313–316.
(8) Li, B.; Wang, L.; Kang, B.; Wang, P.; Qiu, Y. *Sol. Energy Mater. Sol. Cells* **2006**, *90*, 549–573.
(9) Stathatos, E.; Lianos, P.; Lavrencic-Stangar, U.; Orel, B. *Adv. Mater.* **2002**, *14*, 354–357.
(10) Wang, L.; Fang, S.; Lin, Y.; Zhou, X.; Li, M. *Chem. Commun.* **2005**, 5687–5689.
(11) Li, F.; Cheng, F.; Shi, J.; Cai, F.; Liang, M.; Chen, J. *J. Power Sources* **2007**, *165*, 911–915.
(12) Cao, F.; Oskam, G.; Searson, P. C. *J. Phys. Chem.* **1995**, *99*, 17071–17073.
(13) Tu, C.-W.; Liu, K.-Y.; Chien, A.-T.; Lee, C.-H.; Ho, K.-C.; Lin, K.-F. *Eur. Polym. J.* **2008**, *44*, 608–614.
(14) Wu, J.; Lan, Z.; Lin, J.; Huang, M.; Hao, S.; Sato, T.; Yin, S. *Adv. Mater.* **2007**, *19*, 4006–4011.
(15) Wu, J.; Lan, Z.; Wang, D.; Hao, S.; Lin, J.; Wei, Y.; Yin, S.; Sato, T. *J. Photochem. Photobiol. A* **2006**, *181*, 333–337.
(16) Komiya, R.; Han, L.; Yamanaka, R.; Islam, A.; Mitate, T. *J. Photochem. Photobiol. A* **2004**, *164*, 123–127.
(17) Ardo, S.; Meyer, G. J. *Chem. Soc. Rev.* **2009**, *38*, 115–164.
(18) Chen, Z.; Li, F.; Huang, C. *Curr. Org. Chem.* **2007**, *11*, 1241–1258.
(19) Ito, S.; Zakeeruddin, S. M.; Humphry-Baker, R.; Liska, P.; Charvet, R.; Comte, P.; Nazeeruddin, M. K.; Péchy, P.; Takata, M.; Miura, H.; Uchida, S.; Grätzel, M. *Adv. Mater.* **2006**, *18*, 1202–1205.
(20) Kim, S.; Kim, D.; Choi, H.; Kang, M.-S.; Song, K.; Kang, S. O.; Ko, J. *Chem. Commun.* **2008**, 4951–4953.
(21) Liang, M.; Xu, W.; Cai, F.; Chen, P.; Peng, B.; Chen, J.; Li, Z. *J. Phys. Chem. C* **2007**, *111*, 4465–4472.
(22) Xu, W.; Peng, B.; Chen, J.; Liang, M.; Cai, F. *J. Phys. Chem. C* **2008**, *112*, 874–880.
(23) Xu, W.; Pei, J.; Shi, J.; Peng, S.; Chen, J. *J. Power Sources* **2008**, *183*, 792–798.
(24) Shi, J.; Liang, J.; Peng, S.; Xu, W.; Pei, J.; Chen, J. *Solid State Sci.* **2009**, *11*, 433–438.
(25) Ito, S.; Chen, P.; Comte, P.; Nazeeruddin, M. K.; Liska, P.; Péchy, P.; Grätzel, M. *Prog. Photovoltaics* **2007**, *15*, 603–612.
(26) Nazeeruddin, M. K.; Kay, A.; Rodicio, I.; Humpbry-Baker, R.; Müller, E.; Liska, P.; Vlachopoulos, N.; Grätzel, M. *J. Am. Chem. Soc.* **1993**, *115*, 6382–6390.
(27) Wang, Q.; Ito, S.; Grätzel, M.; Fabregat-Santiago, F.; Mora-Seró, I.; Bisquert, J.; Bessho, T.; Imai, H. *J. Phys. Chem. B* **2006**, *110*, 25210–25221.
(28) Wu, J.; Hao, S.; Lan, Z.; Lin, J.; Huang, M.; Huang, Y.; Fang, L.; Yin, S.; Sato, T. *Adv. Funct. Mater.* **2007**, *17*, 2645–2652.
(29) Arunbabu, D.; Sannigrahi, A.; Jana, T. *J. Phys. Chem. B* **2008**, *112*, 5305–5310.
(30) Wu, J.; Lan, Z.; Wang, D.; Hao, S.; Lin, J.; Huang, Y.; Yin, S.; Sato, T. *Electrochim. Acta* **2006**, *51*, 4243–4249.
(31) Choe, H. S.; Carrol, B. G.; Pasquariello, D. M.; Abraham, K. M. *Chem. Mater.* **1997**, *9*, 369–379.
(32) Hauch, A.; Georg, A. *Electrochim. Acta* **2001**, *46*, 3457–3466.
(33) Fabregat-Santiago, F.; Bisquert, J.; Palomares, E.; Otero, L.; Kuang, D.; Zakeeruddin, S. M.; Grätzel, M. *J. Phys. Chem. C* **2007**, *111*, 6550–6560.
(34) Bai, Y.; Cao, Y.; Zhang, J.; Wang, M.; Li, R.; Wang, P.; Zakeeruddin, S. M.; Grätzel, M. *Nat. Mater.* **2008**, *7*, 626–630.
(35) Gao, F.; Wang, Y.; Shi, D.; Zhang, J.; Wang, M.; Jing, X.; Humphry-Baker, R.; Wang, P.; Zakeeruddin, S. M.; Grätzel, M. *J. Am. Chem. Soc.* **2008**, *130*, 10720–10728.
(36) Kuang, D.; Ito, S.; Wenger, B.; Klein, C.; Moser, J.-E.; Humphry-Baker, R.; Zakeeruddin, S. M.; Grätzel, M. *J. Am. Chem. Soc.* **2006**, *128*, 4146–4154.
(37) Nazeeruddin, M. K.; Zakeeruddin, S. M.; Humphry-Baker, R.; Jirousek, M.; Liska, P.; Vlachopoulos, N.; Shklover, V.; Fischer, C.-H.; Grätzel, M. *Inorg. Chem.* **1999**, *38*, 6298–6305.
(38) Zhang, Z.; Zakeeruddin, S. M.; O'Regan, B. C.; Humphry-Baker, R.; Grätzel, M. *J. Phys. Chem. B* **2005**, *109*, 21818–21824.

AM9000375